Materials Today • Volume xxx, Number xx • xxxx 2019

Kirigami-inspired strain-insensitive sensors based on atomically-thin materials

Keong Yong, Subhadeep De, Ezekiel Y. Hsieh, Juyoung Leem, Narayana R. Aluru, SungWoo Nam *

Department of Mechanical Science and Engineering, University of Illinois at Urbana-Champaign, Urbana, IL 61801, United States

This work reports kirigami-inspired architectures of graphene for strain-insensitive, surface-conformal stretchable multifunctional electrodes and sensors. The kirigami-inspired graphene electrode exhibits strain-insensitive electrical properties up to 240% applied tensile strain and mixed strain states, including a combination of stretching, twisting, and/or shearing. Moreover, a multitude of kirigami designs of graphene are explored computationally to predict deformation morphologies under different strain conditions and to achieve controllable stretchability. Notably, strain-insensitive graphene field-effect transistor and photodetection under 130% stretching and 360° torsion are achieved by strategically redistributing stress concentrations away from the active sensing elements via strain-responsive out-of-plane buckling at the vicinity of the kirigami notches. The combination of ultra-thin form factor, conformity on skin, and breathable notches suggests the applicability of kirigami-inspired platform based on atomically-thin materials in a broader set of wearable technology.

Introduction

Recent progress in the fabrication of flexible electronics has enabled various nanomaterials-based flexible devices to be conformal to the skin or even implanted into the human body for continuous monitoring and treatment purposes [1–8]. From the perspective of material development, atomically-thin materials offer tunable properties with enhanced performance over their bulk counterparts [9,10]. Graphene, an atomically-thin layer of hexagonally bonded carbon atoms, has been widely developed for use in next generation flexible optoelectronic, electromechanical, and bioelectronics applications owing to its outstanding electrical, mechanical and optical properties [11–14]. However, the implementation of graphene into a broader set of flexible/stretchable applications has been hindered by its tendency to fail or deviate electrically at small strain [15]. Ultimately, the covalently bonded graphene carbon networks do not provide sufficient energy dissipation mechanisms under mechanical loading [15]. Specifically, the conductance of chemical vapor deposition (CVD) grown graphene transferred onto an elastomeric substrate is preserved and reversible only up to ~6.5% tensile strain [16]. In contrast, the minimally demanded strain tolerance for wearable health-monitoring devices is ~55% based on basic human motions [17].

Retention of device functionalities under high mechanical strain is desirable for applications which are subjected to active strain environments [18]. Previous studies have utilized either integrated nanomaterials in stretchable polymers [17,19,20], pre-strained flexible elastomeric substrates [11,12,21,22], or multi-layered nanomaterials [15,23] to impart mechanical flexibility or stretchability into otherwise low strain limit nanomaterials. However, the resulting variance of electrical signal due to intrinsic piezoresistivity or premature failure modes can lead to unwanted strain dependency for intended applications. While exceptional bendability can be achieved by adopting an ultra-thin form factor or placing the active sensing element in the neutral plane, the sensor may still fail prematurely under tension [9].

* Corresponding author.
E-mail address: Nam, S. (swnam@illinois.edu)

 https://doi.org/10.1016/j.mattod.2019.08.013

Please cite this article in press as: K. Yong et al., Materials Today (2019), https://doi.org/10.1016/j.mattod.2019.08.013

In order to retain functional electrical properties of a device as desired, there is a great need to decouple desired measurement signals from mechanical stretchability induced electrical signal changes. Kirigami, an art of paper cutting, in general has been well established as a template to create materials with reconfigurable morphological responses. In fact, mechanically driven form of three-dimensional (3D) mesostructures by kirigami micro/nanomembranes have demonstrated topographical complexity that significantly exceeds those possible with other schemes [24,25]. Following that, numerous kirigami-inspired applications have been reported such as multidirectional photodetection/imaging systems [26], tunable optical windows [24,27], sun-tracking solar cells [28], stretchable bioprobes [29], smart adhesion [30], and motion detection [31]. As kirigami features generate geometric deformations that dominate the inherent material elasticity, properties and structures of kirigami are controlled by pattern and orientation of these cuts [18,32–37].

In this paper, we report strain-insensitive, surface conformal graphene-based stretchable electrodes and multifunctional devices by adopting kirigami-inspired architectures (Fig. 1). While suspended graphene kirigami has been demonstrated [38], we seek to overcome its limitation to aqueous environments and realize strain-insensitive sensing under mixed strain states. We exploit the ability of kirigami-inspired perforations or notches to tune the stiffness of our devices in order to improve conformity and breathability onto human skin. Furthermore, we carry out systematic investigations of multitude graphene kirigami design to demonstrate controllable stretchability and preserved electrical signals up to 240% uniaxial strain and other mixed strain states. Moreover, the simulated deformability of kirigami unit cells under strain is found to correspond well with experimental observations, thereby promoting the applicability of computational driven design optimization. Finally, we achieve strain-insensitive solution-gated graphene field-effect transistor (FET) and photodetection under high tensile and torsional strain states by strategically redistributing stress concentrations away from the active sensing elements via kirigami notches and an island-bridge motif.

Results and discussions

The architecture of our kirigami-inspired devices is illustrated in Fig. 1a. The monolayer graphene (Fig. S1, Supplementary

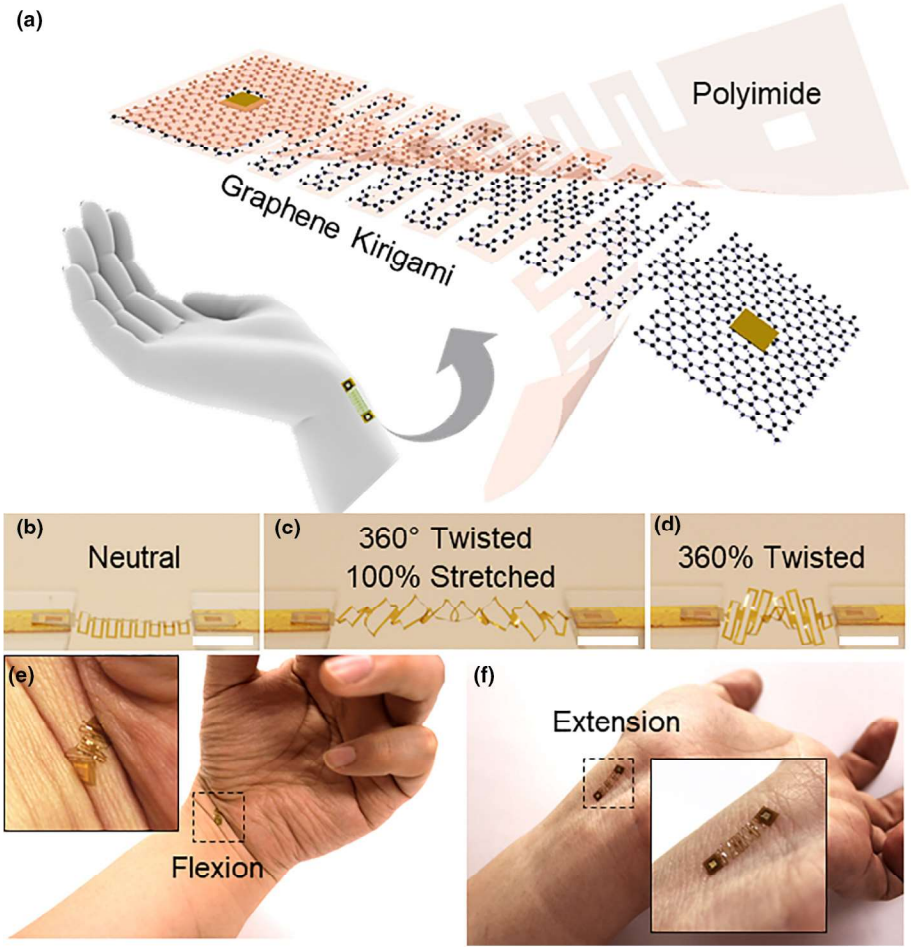

FIGURE 1

Kirigami-inspired architecture for strain-insensitive graphene device. (a) Schematic illustrations of the strain-insensitive graphene electrode. (b–d) Photographs of the kirigami architecture in (b) neutral position, (c) 360° twisted and 100% stretched, and (d) 360° twisted, respectively. Scale bars are 3.5 mm. (e and f) Highly conformal kirigami structures on the surface of a human wrist under (e) flexion and (f) extension articulations, respectively. The insets show the magnified photographs of the delineated regions on the wrist.

Please cite this article in press as: K. Yong et al., Materials Today (2019), https://doi.org/10.1016/j.mattod.2019.08.013

Material) is sandwiched in between two ultrathin polyimide layers (~2–4 μm) and the assembly is patterned into a kirigami shape (Fig. S2). We intended the active sensing element to be in the neutral plane to further minimize the stress subjected to it during deformation. The principle of kirigami is based on patterning the two-dimensional (2D) precursor surface with cuts or notches, where subsequent strain will transform it into a reconfigurable 3D architecture owing to mechanical bistabilty at the vicinity of those patterns. As the kirigami-inspired graphene electrode is stretched uniaxially, the unit cell is subjected to out-of-plane buckling with gradual tilting towards the vertical direction through both bending and twisting accompanied by the widening of unit cell (Video S1, Supplementary Material). Depending on the loading direction, the unit cells will tilt either clockwise or counterclockwise when the kirigami structure is stretched from one end with the other end fixed [34]. The kirigami designs would deform initially in-plane via cut/notch widening, followed by rotation of kirigami beams via hinges [18,32–34]. Further extension causes the in-plane beam bending to become more energetically expensive than out-of-plane beam bending [32,33]. Continued stretching loads the structure until full extension, resulting in strain hardening and ultimately failure [32]. We have also noticed that the strain rate affects the general uniformity and sequence of unit cell widening under mechanical loading. Moreover, the topographical deformation of a kirigami structure is shown to be highly dependent on the applied strain states (Fig. 1b–d), such as mixed tensile and torsional strain (Fig. 1c) or only torsional strain (Fig. 1d). As a preliminary test for structural conformity, we mounted the kirigami architecture on the surface of a human wrist and strained under different wrist articulations, including flexion and extension (Fig. 1e and f). Notably, the perforated/notch kirigami designs further reduced the effective stiffness of the ultrathin form factor structure [32], therefore improving the conformity and breathability of the device, which is conducive to long-term wearable applications [39].

To demonstrate strain-insensitive electrical measurements, we characterized the normalized change in resistance ($\Delta R/R_0$) of a kirigami-inspired graphene electrode under varying types of strain states (Fig. 2). As the graphene electrode is stretched uniaxially from 0% to 240%, there is a negligibly small change (<0.25%) in resistance (Fig. 2a) even when the unit cells are drastically widened. The stable electrical signal is also observed when the graphene electrode is twisted up to two full revolutions or 720° as manifested by the structural distortion in the middle region (Fig. 2b). In addition, we demonstrated time-stable electrical signal preservation under mixed strains states by subjecting the graphene electrode to a combination of uniaxial strain, torsion strain, and/or shear strain, reflecting active working conditions (Fig. 2c).

Mechanical robustness throughout recurring deformations is another important design consideration for wearable devices. To demonstrate the robustness of our stretchable graphene electrode, we characterized the normalized change in resistance over ten thousand periods of cyclic uniaxial tensile strains, between 0% and 120% (Fig. 2d). Notably, no degradation of the normalized resistance was observed over such a large number of stretching/releasing cycles, implying that the graphene kirigami's integrity is preserved during the cyclic motion.

In contrast to kirigami-inspired architecture, the crumpling of atomically thin materials has similarly been reported to enhance device stretchability [12,22,40]. Given the shared attributes of topography engineering, we characterized the normalized change of resistance as a function of strain for a crumpled

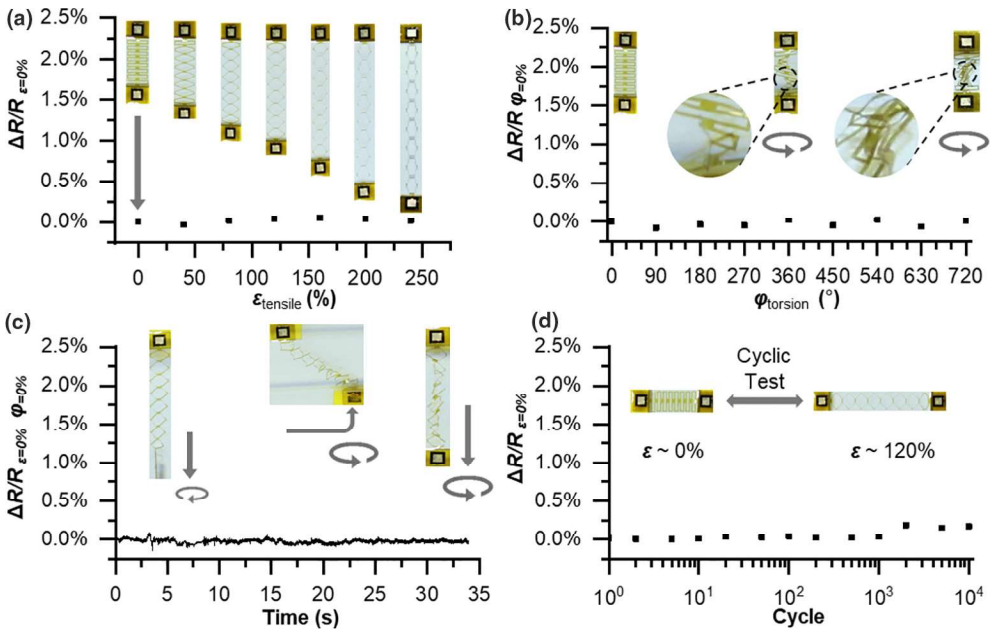

FIGURE 2

Strain-insensitive electrical measurements of a kirigami-inspired graphene electrode under different strain states. The strain-insensitive electrical measurement is conducted under (a) uniaxial strain ranging from 0 to 240%; (b) torsion strain up to 720° or two full revolutions; (c) mixed strain states including uniaxial strain, torsion, and shear; and (d) cyclic stretching between 0% and 120% up to 10,000 cycles.

Please cite this article in press as: K. Yong et al., Materials Today (2019), https://doi.org/10.1016/j.mattod.2019.08.013

graphene electrode. As the buckle-delaminated graphene electrode on elastomeric substrate is stretched up to ~200% uniaxially, we measured a ~25% change in normalized resistance (Fig. S3), which is >100 times larger than the recorded resistance change by kirigami-inspired graphene electrode (Fig. 2a). Even though the pre-strained value (350%) of the elastomeric substrate is much larger than the applied strain, the variance in resistance under mechanical loading suggests its susceptibility to strain effects.

To evaluate the case in which out-of-plane deformation is limited, we adhered the kirigami-inspired graphene electrode onto an elastomeric very high bond (VHB) substrate (Fig. S4). The setup effectively constrained the out-of-plane deformation of the kirigami electrode under any mechanical loading, thereby diminishing the stress alleviation thereof. As the restricted kirigami electrode was uniaxially stretched, the normalized resistance changed monotonically when compared to the strain-insensitive unconstrained setup (Figs. 2 and S4).

To extend the strain-insensitivity scheme to another compliant substrate material, we utilized polydimethylsiloxane (PDMS). Given the incompatibility of PDMS with the proposed microfabrication procedures (e.g., swelling by organic solvent), we used a laser cutter to pattern the kirigami design of the sandwiched architecture and to highlight the potential versatility of a new kirigami patterning scheme (Fig. S5). As the kirigami electrode was uniaxially stretched under smaller strains (below 50%), the normalized resistance remained unchanged. The level of strain insensitivity exhibited by kirigami-inspired PDMS structures was better than that of crumpled graphene structures (gauge factor ~0.033 between 0 and 80%) (Fig. S3) and restricted kirigami-inspired polyimide structures (gauge factor ~0.026 between 0–60%) (Fig. S4). Further extension of the kirigami-inspired PDMS structure indicated monotonic increment in normalized resistance (e.g., gauge factor ~0.050 above 50%).

To predict the morphology of a kirigami-inspired structure under strain, we used finite element analysis (FEA) to simulate the polyimide strain-responsive architecture without accounting for graphene given the significant thickness difference (Fig. 3). Side view photographs of graphene kirigami electrode are investigated to study the evolution of morphology under increasing uniaxial strain (Fig. 3a–c). The general correspondence between experimental observations (Fig. 3a–c) and simulated results (Fig. 3d–f) with respect to the deformity of kirigami unit cells established simulation as a means for computationally driven design optimization, as suggested subsequently in the engineering of multifunctional kirigami devices. Quantitative agreement of the experimental configuration states of 8 kirigami edges (or 4 kirigami unit cell) with FEA predictions of *z*-displacements under

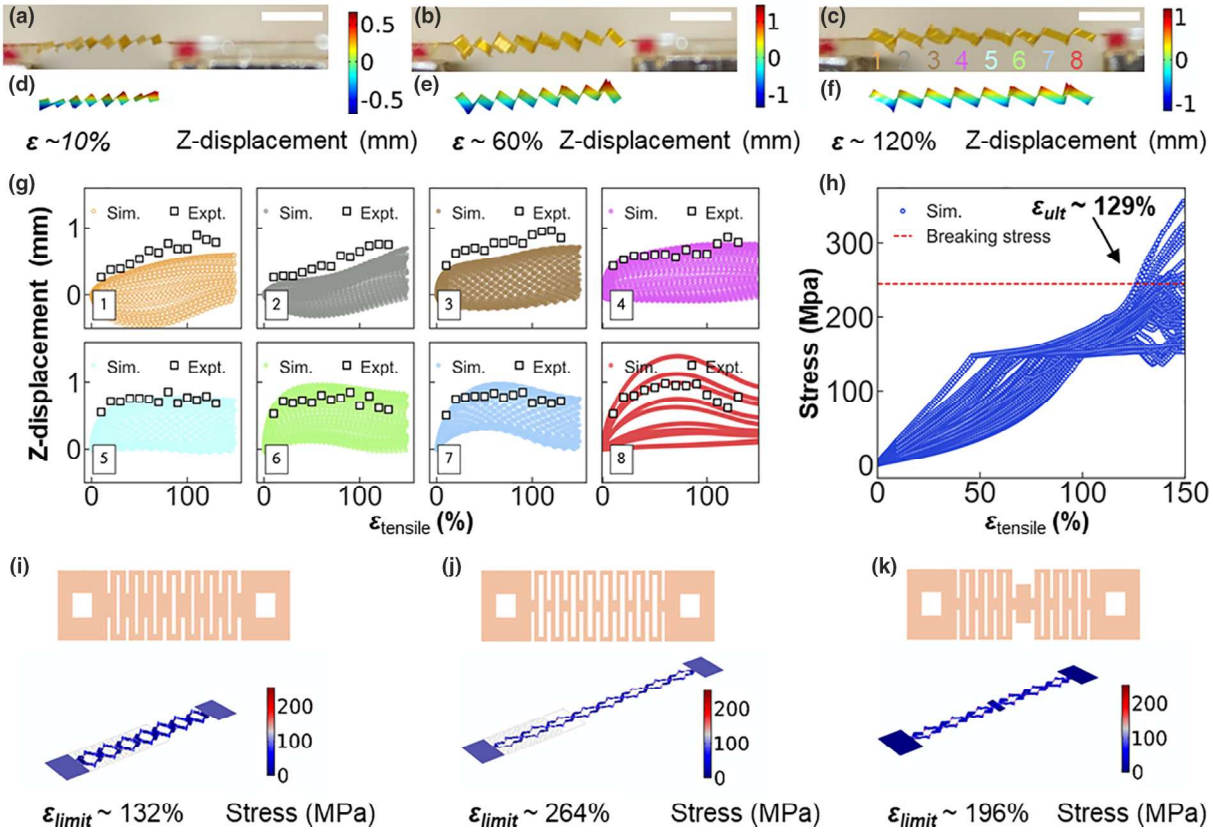

FIGURE 3

Finite element analysis (FEA) of a kirigami-inspired graphene structure under strain. (a–c) Photographs of side view graphene electrode with increasing uniaxial tensile strain from 10% to 120%. Scale bar is 2 mm. (d–f) Simulated results corresponding the strain effect for a–c on the graphene electrode. (g) Experimental observations and simulated results for *z*-displacement of the 8 kirigami edges (4 kirigami unit cells shown in Fig. S6b) as numbered in c. (h) Simulated stress values at the edges of kirigami notches and the corresponding breaking/ultimate stress. (i–k) FEA analysis illustrating the stress distribution and uniaxial strain limit of different kirigami designs.

Please cite this article in press as: K. Yong et al., Materials Today (2019), https://doi.org/10.1016/j.mattod.2019.08.013

increasing tensile strain (0–120%) is presented in Figs. 3g and S6a–c.

Moreover, FEA can also reveal the distribution of stress in a kirigami structure, thus providing insights into the ability of kirigami to redistribute stress concentrations within a structure (Fig. S6d and e). Conveniently by a computational mean, we predicted the uniaxial strain limit of specific kirigami designs by corresponding the ultimate/breaking stress to the stresses at the vicinity of the notches (Figs. 3h and S6d and e). We captured the strain-responsive complex out-of-plane bending and twisting by studying the evolution of unit cell morphology under linear stretching motions (Fig. S6f–h). The kirigami architecture becomes reconfigured under strain, with maximum stresses occurring at the regions with the highest change in curvature, and these regions remained constant throughout the buckling process (Fig. S6f–h). Following that, the surface strain distribution of a twisted kirigami indicated both tension and compression at localized regions (Fig. S7). The deterministic stress distributions validated our approach to mitigate stresses away from active sensing element and towards the vicinity of patterned notches. However, interfacial stress transfer may lead to shear sliding under tension and buckling under compression above the corresponding critical strains in the graphene kirigami at large deformations [41].

A multitude of kirigami designs with varying notch length, beam width, hinge length, number of notches, number of rows, and thickness were evaluated for their strain limit and corresponding morphology (Fig. S8). As we evaluated different notch designs (Figs. 3i–k and S8), we found that notch length, hinge length and beam width play critical roles in determining the stretchability of a specific kirigami design. The control of beam width, reflected by the change of notch width, represents an effective approach to tune the directional stretchability of explored kirigami designs (Fig. S8a and b). Increasing notch length or decreasing beam width (and hinge length) lowers the critical force needed to buckle out-of-plane. The out-of-plane deformation redistributes the stress concentrations to the vicinity of patterned notches (Figs. S6e and S8) which affords the kirigami structure to withstand higher overall applied strain (stretchability). On the other hand, we found that thickness of polyimide in the scale of interest (4–40 μm) yielded little variance in effective uniaxial strain limit (Fig. S8b). Essentially, there is a general tradeoff between structure stretchability and mechanical rigidity appreciated for device handling. Our range of evaluated designs implied controllable stretchability enabled by kirigami architecture engineering.

Impermeable ultrathin films or rubber sheets, as demonstrated by previous studies, may disturb sweat secretion and block airflow around the skin, causing irritation and inflammation, which may ultimately lead to lasting physiological and psychological effects [39]. In contrast, kirigami-inspired architectures have the potential to improve the breathability of skin electronic devices by reducing the relative area coverage and through out-of-plane deformation (Figs. S9 and 1e and f). However, the relationship between surface area and uniaxial stretchability is found to be neither linear nor monotonic, but instead, more design dependent. In the case of preserved overall dimensions (e.g., length, width, and thickness), directional mechanical stiffness can be tuned by modulating the number of kirigami rows without compromising breathability (Fig. S9). Our skin mounting demonstrations showed potential applications in skin wear electronics, where conformity and breathability are appreciated.

To substantiate the implications for strain-insensitive applications, we investigated solution-gated FET and photodetection enabled by kirigami-inspired architecture (Fig. 4). A kirigami design with an island-bridge motif is chosen for the dual function device platform (Fig. 4a). As we explored different island designs, we found that drastic improvement in stretchability was found by reducing island width and hinge length (Fig. S8c). By introducing strategic notches, kirigami now provides a distinct route to locally relieve stresses through these geometric features (Fig. 4b). Suppression of strain profile around the active sensing region is critical to strain-insensitive performance of flexible/stretchable devices.

Solution-gated FET plays a crucial role in chemical and biological sensing applications for enabling electrical signal transduction and amplification. Correspondingly, there is a growing interest into in-situ perspiration analysis among skin electronic devices, namely sweat metabolites such as glucose and lactate, as well as electrolytes such as sodium and potassium ions [5]. The working principal of our solution-gated FET is based on applying gate potential via the electric double layer (EDL) on the surface of graphene channel, which results in the modulation of graphene conductance. The stretchable solution-gated graphene kirigami FET device consisted of gold electrodes as the source and drain contacts and an exposed graphene channel in phosphate-buffered saline (PBS) solution (Fig. 4c). For a gate sweep between −0.2 V and 0.6 V using Ag/AgCl reference electrode, we observed ambipolar field-effect gating (Fig. 4e), with *p*- and *n*-type normalized transconductance, g_{mN} of −1.13 and 0.90 mS/V (Fig. S10a), respectively, comparable to reported device performance of flat graphene on flexible polymeric substrate [42]. Notably, we demonstrated strain-insensitive transfer curves (Fig. 4e) and transconductance characteristics (Fig. S10a) across all three different structural configurations: neutral, 130% uniaxial strain, and 360° torsional strain enabled by kirigami architecture. Similar levels of strain insensitivity were observed for all-graphene FETs (i.e., extended Au source and drain electrodes are removed) between their neutral state and 150% uniaxial strain (Fig. S11).

Moreover, we have explored an integrated planar gate electrode design to further close the practicality gap of solution-gated FET sensing (Fig. S12). While there are small discrepancies in the transfer curve characteristics between the Ag/AgCl reference gate electrode and the planar Au gate electrode, strain-insensitivity was demonstrated between 0% and 150% uniaxial strain. The demonstration of kirigami graphene FET has the potential to be extended to health monitoring applications.

In addition, the same device platform and structural configurations are also extended to photodetection (Fig. 4d) under green laser illumination. Photodetection is an integral part of noninvasive heart rate monitoring or photoplethsmography (PPG) by monitoring light absorption caused by variations in blood volume passing through arteries [43]. Our photodetector is based

Please cite this article in press as: K. Yong et al., Materials Today (2019), https://doi.org/10.1016/j.mattod.2019.08.013

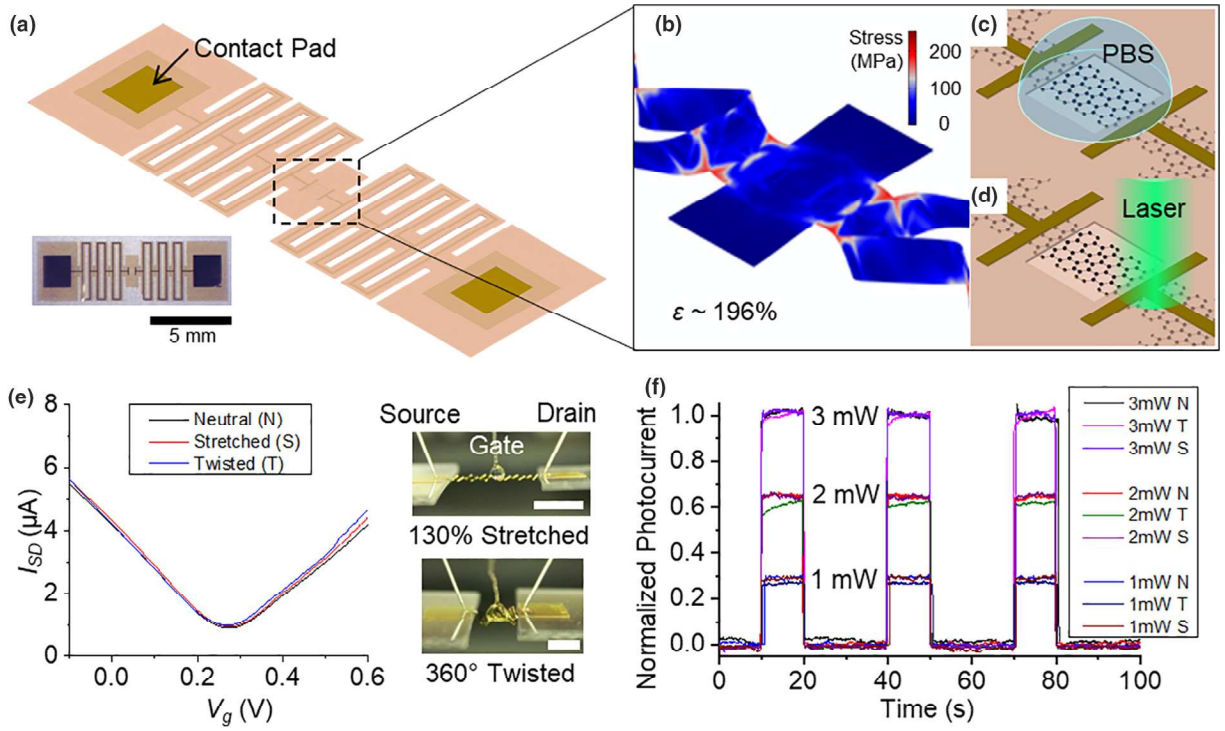

FIGURE 4

Kirigami-inspired strain-insensitive multi-functional graphene devices. (a) Schematic illustrations of the kirigami design chosen for sensing application. Inset shows the photograph of the actual device. (b) FEA simulation results on the stress distribution of the center island and the nearby notches at ~196% uniaxial strain. (c and d) Schematic illustrations of PBS-gated FET sensing and photodetection, respectively. (e) Strain-insensitive ambipolar transfer curves of the PBS-gated graphene FET under 3 structural configurations. Photographs show the experimental configuration of PBS-gated FET under stretching and twisting. Scale bar is 5 mm. (f) Normalized photocurrent (by photocurrent value measured with the incident laser power of 3 mW) of the graphene photodetector under 3 structural configurations and laser power ranging from 1 to 3 mW. N denotes neutral, T denotes 130% stretched, and S denotes 360° twisted.

on the separation of photogenerated electron-hole pairs under an electric field sustained by applied bias voltage [44]. The green laser is illuminated at the junction of graphene channel and gold electrode to maximize photocurrent generation [45]. We demonstrated strain-insensitive photodetection by measuring photocurrent generation with three varying laser powers (1–3 mW) under different structural configurations (Figs. 4f and S10b). For each laser power, we observed dynamic photoresponse of time-varying photocurrent with the laser turned on (~10 s) and off (~20 s) for all structural configurations (neutral, N; stretched, S; and twisted, T). The measured photocurrents are normalized to the photocurrent measured at 3mW laser power. Our strain-insensitive normalized photocurrent successfully demonstrated that our kirigami-inspired structure with an island-bridge motif provided stable photodetection under distorted configurations (Fig. 4f). Our kirigami-inspired solution-gated FET and photodetection further implied the potential for multifunctional wearables complemented by surface conformity and general breathability.

Conclusion

We have demonstrated that engineering of graphene device deformability via kirigami architecture has the potential to achieve strain-insensitive electrical sensing. The kirigami-inspired graphene architectures exhibited controllable stretchability and preserved electrical signals up to 240% uniaxial stretching and other strain states. In addition, the kirigami-inspired perforations and notches improved conformity and breathability by tuning the stiffness of the system. In addition, FEA simulation of kirigami architecture suggested the applicability of computationally driven design optimization to strain-responsive structural reconfiguration. More notably, we achieved strain-insensitive solution-gated graphene FET and photodetection under stretching and torsion by strategically redistributing stress concentrations away from the active sensing elements via kirigami notches and an island-bridge motif. We believe that the kirigami-inspired strain-insensitive design template presented a simple and robust platform which is applicable to a wide range of other atomically thin materials of recent interest (e.g., hBN, MoS_2, and other transition metal dichalcogenides). Our research will allow for the realization of enhanced stretchability, strain-insensitive, surface-conformal and breathable skin electronics. The kirigami-inspired highly stretchable architecture also has the future potential for multifunctional sensor integrations demanded in wearable health monitoring applications.

Materials and methods

Kirigami device fabrication

Graphene is synthesized on copper foil by low-pressure CVD using a mixture of methane (CH_4), hydrogen (H_2), and argon (Ar). The first or bottom polyimide layer is spincoated and cured on a sacrificial metal layer. The graphene is subsequently

Please cite this article in press as: K. Yong et al., Materials Today (2019), https://doi.org/10.1016/j.mattod.2019.08.013

transferred on top of the assembly and annealed to enhance the adhesion. Metal electrodes are deposited before the graphene is patterned by photolithography and oxygen (O_2) plasma. Following that, the second or top polyimide layer is then spincoated and cured. The assembly is then patterned into a kirigami shape by reactive ion etching (RIE) after etch mask deposition. Finally, the device is released by etching the sacrificial layer chemically. The detailed procedures and conditions during sample preparation, e.g., graphene synthesis, sample preparation for buckle-delaminated crumpled graphene, etc., are provided in Supplementary material.

Electrical characterizations

Two terminal resistance measurements are performed with a probe station (PM8, SUSS Micro Tec, Germany) and a sourcemeter (2614B, Keithley Instruments, OH). The current–voltage curve of the kirigami-inspired graphene devices are characterized at varying strain states.

Cyclic uniaxial tensile test

The kirigami-inspired graphene electrode is mounted on top of an automatic translational stage (MTS50-Z8, Thorlabs, NJ) interfaced with a brushed motor controller. The cyclic uniaxial tensile test is run at a maximum velocity of 1.5 mm/s with an acceleration of 1.5 mm/s^2.

Finite element modeling

Non-linear finite element (FE) analysis is carried out to predict the mechanical response of various kirigami designs using the Structural Mechanics Module in COMSOL Multiphysics® software. The non-linear treatment is essential due to large displacements and rotations involved with the kirigami deformation. A 3D solid element is employed to model the kirigami structures. A triangular prism non-uniform meshing is used with maximum and minimum mesh size of ~1.3 mm and ~0.096 mm, respectively. The discretization is verified by checking simulation results with smaller mesh sizes. For the polyimide material of the kirigami, an elasto-plastic constitutive model is adopted [46]. The FE simulation involved two steps. First, very small perturbative forces are applied in the out-of-plane direction along the top edges of the cuts while keeping the ends of the kirigami fixed to prevent bifurcation during buckling transition [24]. Next, the axial loading is imposed by moving one end along the plane in steps, and the increments are kept small enough to ensure the convergence of the non-linear problem.

We have also developed a supplementary open source web-based kirigami simulation design and mechanical assist tool to assist computationally-driven morphology prediction of kirigami structure under strain, GAMIAN (website: https://nanohub.org/-tools/gamian). The details are provided in the Supplementary information.

FET sensor measurements

Solution-gated FET transfer curves are measured with a digital sourcemeter (2614B, Keithley Instruments, OH) with an Ag/AgCl reference electrode (Harvard Instruments, MA) to gate the device through 1× PBS solution (Corning Cellgro, VA). The gate voltage is swept from −0.2 V to 0.6 V, while the bias voltage is kept at 30 mV.

Photocurrent measurements

The photocurrent of the device generated by the incident beam from a diode laser of 515 nm wavelength (power ~1–3 mW through a 5× objective lens) (CPS532, Thorlabs, NJ) is measured using a sourcemeter (Keithley 2614B, OR) and a microprobe station. To maintain a consistent power and illumination position, the laser power and beam focus/alignment is calibrated through a 5× objective lens with a photodiode power sensor (S120C and PM100USB, Thorlabs, NJ). The bias voltage of 15 μV is applied for the electrical potential.

Acknowledgements

S.N. gratefully acknowledges support from the NSF (EEC-1720701, CMMI-1554019 and MRSEC DMR-1720633), AFOSR/AOARD (FA2386-17-1-4071 and FA9550-16-1-0251), ARL (W911NF-16-2-0220), NASA ECF (NNX16AR56G), ONR YIP (N00014-17-1-2830) and JITRI. Experiments are carried out in part in the Materials Research Laboratory Central Research Facilities, Holonyak Micro & Nanotechnology Laboratory, and the Beckman Institute Imaging Technology Group at the University of Illinois at Urbana-Champaign. This research was partially supported by the NSF through the University of Illinois at Urbana-Champaign Materials Research Science and Engineering Center DMR-1720633.

Data availability

The raw/processed data required to reproduce these findings cannot be shared at this time as the data also forms part of an ongoing study.

Appendix A. Supplementary data

Supplementary data to this article can be found online at https://doi.org/10.1016/j.mattod.2019.08.013.

References

[1] W.A.D.M. Jayathilaka et al., Adv. Mater. 31 (2019) 1805921.
[2] K. Kang, Y. Cho, K.J. Yu, Micromachines 9 (2018) 263.
[3] Y.J. Hong et al., Adv. Funct. Mater. 29 (2019) 1808247.
[4] Y.J. Park et al., ACS Nano 13 (2019) 3023–3030.
[5] W. Gao et al., Nature 529 (2016) 509–514.
[6] S. Kabiri Ameri et al., ACS Nano 11 (2017) 7634–7641.
[7] S. Xu et al., Science 344 (2014) 70–74.
[8] S.K. Kang et al., Nature 530 (2016) 71–76.
[9] D. Akinwande, N. Petrone, J. Hone, Nat. Commun. 5 (2014) 5678.
[10] K.S. Novoselov et al., Nature 490 (2012) 192–200.
[11] K. Yong et al., Sci. Rep. 6 (2016) 24890.
[12] P. Kang et al., Adv. Mater. 28 (2016). 4565–4565.
[13] M.C. Wang et al., 2D Mater. 4 (2017).
[14] P. Kang, M.C. Wang, S. Nam, Microelectron. Eng. 161 (2016) 18–35.
[15] N. Liu et al., Sci. Adv. 3 (2017) e1700159.
[16] K.S. Kim et al., Nature 457 (2009) 706–710.
[17] T. Yamada et al., Nat. Nanotechnol. 6 (2011) 296–301.
[18] T.C. Shyu et al., Nat. Mater. 14 (2015) 785–789.
[19] Y. Zhang et al., Adv. Mater. 22 (2010) 3027–3031.
[20] Y. Kim et al., Nature 500 (2013) 59–63.
[21] J. Zang et al., Nat. Mater. 12 (2013) 321–325.
[22] M. Kim, P. Kang, J. Leem, S.W. Nam, Nanoscale 9 (2017) 4058–4065.
[23] S. Won et al., Nanoscale 6 (2014) 6057–6064.
[24] Y. Zhang et al., Proc. Natl. Acad. Sci. U.S.A. 112 (2015) 11757–11764.
[25] S. Xu et al., Science 347 (2015) 154–159.

Please cite this article in press as: K. Yong et al., Materials Today (2019), https://doi.org/10.1016/j.mattod.2019.08.013

[26] W. Lee et al., Nat. Commun. 9 (2018) 1417.
[27] Z. Liu et al., Sci. Adv. 4 (2018). eaat4436.
[28] A. Lamoureux et al., Nat. Commun. 6 (2015) 8092.
[29] Y. Morikawa et al., Adv. Healthc. Mater. 7 (2018) 1701100.
[30] D.G. Hwang, K. Trent, M.D. Bartlett, ACS Appl. Mater. Interfaces 10 (2018) 6747–6754.
[31] W. Zheng et al., Chem. Mater. 30 (2018) 6063–6070.
[32] D.G. Hwang, M.D. Bartlett, Sci. Rep. 8 (2018) 3378.
[33] M. Isobe, K. Okumura, Sci. Rep. 6 (2016) 24758.
[34] A. Rafsanjani, K. Bertoldi, Phys. Rev. Lett. 118 (2017) 084301.
[35] Y. Cho et al., Proc. Natl. Acad. Sci. U.S.A. 111 (2014) 17390–17395.
[36] Y. Tang et al., Adv. Mater. 29 (2017) 1604262.
[37] Y. Tang et al., Adv. Mater. 27 (2015) 7181–7190.
[38] M.K. Blees et al., Nature 524 (2015) 204–207.
[39] A. Miyamoto et al., Nat. Nanotechnol. 12 (2017) 907–913.
[40] J. Leem et al., Nano Lett. 15 (2015) 7684–7690.
[41] T. Jiang, R. Huang, Y. Zhu, Adv. Funct. Mater. 24 (2014) 396–402.
[42] B.J. Kim et al., Nano Lett. 10 (2010) 3464–3466.
[43] Y. Wang, Z. Liu, B. Dong, Proc. Annu. Int. Conf. IEEE Eng. Med. Biol. Soc. EMBS (2016) 3511–3514.
[44] F.H.L. Koppens et al., Nat. Nanotechnol. 9 (2014) 780–793.
[45] F. Xia et al., Nat. Nanotechnol. 4 (2009) 839–843.
[46] W.Y. Chang, T.H. Fang, Y.C. Lin, Appl. Phys. A: Mater. Sci. Process. (2008) 693–701.

Please cite this article in press as: K. Yong et al., Materials Today (2019), https://doi.org/10.1016/j.mattod.2019.08.013